First-principles thermoelasticity of transition metals at high pressure: Tantalum prototype in the quasiharmonic limit

Daniel Orlikowski, Per Söderlind, and John A. Moriarty
Lawrence Livermore National Laboratory, University of California, P.O. Box 808, Livermore, California 94551-0808, USA
(Received 26 April 2006; revised manuscript received 13 July 2006; published 23 August 2006)

The thermoelastic properties of tantalum have been investigated over its theoretical high-pressure bcc solid phase (up to 26 000 K at 10 Mbar) using an advanced first-principles approach that accurately accounts for cold, electron-thermal, and ion-thermal contributions in materials where anharmonic effects are small. Specifically, we have combined *ab initio* full-potential linear-muffin-tin-orbital electronic-structure calculations for the cold and electron-thermal contributions to the elastic moduli with phonon contributions for the ion-thermal part calculated using model generalized pseudopotential theory. For the latter, a summation of terms over the Brillouin zone is performed within the quasiharmonic approximation, where each term is composed of a strain derivative of the phonon frequency at a particular **k** point. At ambient pressure, the resulting temperature dependence of the Ta elastic moduli is in excellent agreement with ultrasonic measurements. The experimentally observed anomalous behavior of C_{44} at low temperatures is shown to originate from the electron-thermal contribution. At higher temperatures, the main contribution to the temperature dependence of the elastic moduli comes from thermal expansion, but inclusion of the electron- and ion-thermal contributions is essential to obtain quantitative agreement with experiment. In addition, the pressure dependence of the moduli at ambient temperature compares well with recent diamond-anvil-cell measurements to 1.05 Mbar. Moreover, the calculated longitudinal and bulk sound velocities in polycrystalline Ta at higher pressure and temperature in the vicinity of shock melting (~3 Mbar) agree well with data obtained from shock experiments. However, at high temperatures along the melt curve above 1 Mbar, the B' shear modulus becomes negative, indicating the onset of unexpectedly strong anharmonic effects. Finally, the assumed temperature dependence of the Steinberg-Guinan strength model obtained from scaling with the bulk shear modulus is examined at ambient pressure.

DOI: 10.1103/PhysRevB.74.054109 PACS number(s): 46.25.Hf, 62.20.Dc, 74.25.Ld, 63.10.+a

I. INTRODUCTION

Vital to the understanding of the mechanical properties of metals is the multiscale linkage between atomic-level elastic and defect properties[1] and continuum-level constitutive models, such as the well-known Steinberg-Guinan and Steinberg-Lund strength models.[2] One fundamental link between these length scales is the single-crystal elastic moduli, which on the one hand are determined at the atomic level from quantum mechanics, while on the other hand, when suitably averaged, they are also observed to provide both pressure and temperature scaling of the macroscopic yield strength, as indeed is assumed in most of the continuum-level models. Experimentally, the elastic moduli in typical bcc metals such as tantalum (Ta) are observed to stiffen under the application of pressure,[3] but to soften as the temperature increases.[4,5] Modern electronic-structure methods based on density functional theory[6] (DFT) can treat the zero-temperature pressure dependence of single-crystal elastic moduli from first principles,[7,8] and in the case of Ta these have been predicted all the way to 10 Mbar in pressure. Treating the corresponding temperature dependence, and more generally the full temperature-pressure thermoelasticity, is a more formidable challenge, however. In this regard, there has been recent work on new approaches to thermoelasticity for metals with applications to simple metals [Mg (Ref. 9)] and to transition metals [Ta (Ref. 10)]. Here we present an alternative first-principles method relevant to transition metals with small anharmonic effects, which is expected to include the group-VB bcc metals V, Nb, and Ta,[11] at least near ambient pressure. We are also currently extending our approach to include anharmonic effects, and this extension will be reported in a subsequent second paper in this series.

The present focus on Ta is motivated by several additional factors as well. First, this metal is a prototype *d*-transition metal for high-pressure investigations, with a high melting temperature and a single solid bcc phase stable over a wide range of pressure,[12] which makes it a good candidate for both equation of state and materials strength calibration. Tantalum has also been a recent favorite bcc metal for advanced methodology development aimed at structural and thermodynamic properties as well as elasticity, defects, and the multiscale modeling of mechanical properties.[1,7,10,13–16] In this regard, Ta shares in common with other central transition metals the challenging physics issues of (i) directional *d*-electron bonding, requiring robust electronic-structure methods and an accurate treatment of angular as well as radial interatomic forces, and (ii) a high density of electronic states near the Fermi level and significant electronic excitation at high temperatures, requiring an explicit treatment of electron-thermal as well as ion-thermal contributions to thermodynamic and mechanical properties.

The electron-thermal contribution to thermoelasticity in transition metals can be treated in a reasonably straightforward manner by extending cold or zero-temperature DFT electronic-structure calculations of elastic moduli to finite temperature.[10,13] To treat the ion-thermal contribution, however, one must additionally address the more difficult issue of phonons and their strain dependence at arbitrary temperatures and pressures. Three contrasting current approaches to

 ©2006 The American Physical Society

the latter ion-thermal contribution to thermoelasticity can be identified: (i) Monte Carlo (MC) simulation with exact fluctuation formulas, as have been recently elaborated for simple metals[9]; (ii) cell-model treatments of lattice vibrations, such as the particle-in-a-cell (PIC) model of Gülseren and Cohen[10]; and (iii) the quasiharmonic (QH) phonon formalism of Wallace,[17] as will be used in the present work.

The MC simulation approach is very general but requires an explicit and differentiable representation of the total energy of the system. This is possible for both simple and transition metals using first-principles DFT-based generalized pseudopotential theory (GPT).[18] For the limiting case of simple metals, where both angular forces and electron-thermal contributions can be neglected, the MC approach has been implemented with GPT interatomic potentials and applied to hcp and bcc Mg at high pressures and temperatures.[9] We are also currently extending this approach to bcc transition metals using model-GPT (MGPT) multi-ion potentials,[13,19] as will be reported in our subsequent second paper in this series. The principal advantage of the MC method is that it exactly accounts for anharmonic ion effects through rigorous fluctuation formulas that incorporate all internal relaxations. At the same time, the MC method is computationally very intensive, so there remains considerable interest in less expensive approaches, especially for cases where anharmonic effects are small.

The PIC model of Gülseren and Cohen[10] replaces the full phonon problem with that of a single vibrating ion moving in a cage defined by its frozen neighbors. This permits the incorporation of anharmonic effects at some level of approximation, although the accuracy of this approach is not known *a priori*. The principal advantage of the PIC model is that it is simple enough to be coupled directly to a DFT pseudopotential electronic-structure method employed in a supercell geometry, and the ion-thermal contribution to thermoelasticity can be calculated self-consistently as a function of temperature and pressure without the introduction of any additional parameters. Nonetheless, this too is a rather computationally intensive procedure. The remaining cold and electron-thermal contributions to the elastic moduli are obtained using the full-potential, linearized augmented-plane-wave (FP-LAPW) electronic-structure method. Gülseren and Cohen have used their approach to study high-temperature effects on the elastic moduli of Ta up to 4 Mbar in pressure.[10]

Our present approach to thermoelasticity in bcc transition metals combines two computational techniques: the full-potential, linear-muffin-tin-orbital (FP-LMTO) electronic-structure method as developed by Wills and collaborators[20] and the MGPT interatomic-potential method.[13,19] These methods have been closely linked and used in tandem to treat successfully a wide range of structural, thermodynamic, defect, and mechanical properties of bcc transition metals, with Ta as a prototype.[13] The MGPT multi-ion potentials for Ta well reproduce most relevant zero-temperature properties that can be calculated with the FP-LMTO method. Here MGPT is used to obtain the ion-thermal component of the thermoelasticity, while the FP-LMTO method is used to calculate the cold and electron-thermal components. To obtain the ion-thermal component, MGPT multi-ion potentials have been directly implemented in the QH phonon formalism of Wallace.[17] The advantages of the QH-MGPT approach are principally twofold. First, this method is orders of magnitude less computationally demanding than either MC simulation or the self-consistent PIC model. Second, for any given material the QH-MGPT approach provides a very useful base line for any further investigations of anharmonic effects, as could be accomplished, for example, through MC-MGPT simulation. Our approach has been used to investigate the temperature dependence of the elastic moduli in bcc Ta. That is for all temperatures and pressures below the theoretical melt line, which extends from $T=3\ 400$ K at $P=0$ Mbar to $T=26\ 000$ K at $P=10$ Mbar.[13] As discussed below, our results compare reasonably well (to within about 10%) with available static experimental data for temperatures up to melt[4,5,21] and for high pressures to 1.05 Mbar.[3] In addition, for polycrystalline Ta at more extreme conditions our calculated aggregate sound velocities agree well with available dynamic shock compression experiments.[22] At the same time, we find evidence of increasingly strong anharmonic effects near melt above 1 Mbar. To make a connection to constitutive strength models, we also compare our calculated average shear modulus with results obtained from the Steinberg-Guinan strength model.[2]

In Sec. II, the present formalism for bcc-metal thermoelasticity in the quasiharmonic limit is presented along with the specifics regarding our computational approach. In Sec. III, we present and compare our calculated results for Ta with available experimental data and then we summarize our work and draw conclusions in Sec. IV.

II. QUASIHARMONIC FORMALISM AND COMPUTATIONAL APPROACH

A. Thermoelasticity at high temperature and pressure

In this section, we discuss the present QH formalism and the computational details that compose our calculation of the temperature and pressure dependence of single-crystal elastic moduli in bcc transition metals. In the usual way and following Moriarty *et al.*,[13] the Helmholtz free energy A for a metal at volume Ω and temperature T can be written as a sum of cold, electron-thermal, and ion-thermal contributions:

$$A(\Omega,T) = E_0(\Omega) + A_{\rm el}(\Omega,T) + A_{\rm ion}(\Omega,T), \qquad (1)$$

where E_0 is the zero-temperature total energy of the electronic ground state—i.e., here the frozen bcc lattice; $A_{\rm el}$ represents the electron-thermal contribution from finite-temperature electrons; and $A_{\rm ion}$ represents the ion-thermal contribution arising from ion motion—i.e., bcc phonons—at the same temperature. Here Ω is taken as the volume per atom or atomic volume and A is the free energy per atom. The total hydrostatic pressure in the metal is

$$P(\Omega,T) = -\left.\frac{\partial A(\Omega,T)}{\partial \Omega}\right|_T, \qquad (2)$$

with corresponding relations for its three components. Other thermodynamic quantities and their components are defined similarly.

For the electron-thermal free energy, temperature is incorporated into $A_{\rm el}=E_{\rm el}-TS_{\rm el}$ through (i) self-consistent changes in the electronic density of states (DOS), $n(\epsilon,\Omega,T)$; (ii) a broadened occupation of the DOS via the Fermi-Dirac distribution function $f(\epsilon,T)$; and (iii) the electronic entropy

$$S_{\rm el}(\Omega,T)=-k_B\int d\epsilon\, n(\epsilon,\Omega,T)\{f(\epsilon,T)\ln[f(\epsilon,T)] - [1-f(\epsilon,T)]\ln[1-f(\epsilon,T)]\}. \quad (3)$$

Changes in the DOS and its occupation can arise both from the effects of temperature for fixed structure and from structural disorder due to ion motion. We consider only the former here and evaluate all electron-thermal contributions for the perfect bcc lattice.

In general, the ion-thermal free energy has both quasiharmonic and anharmonic components:

$$A_{\rm ion}(\Omega,T)=A_{qh}(\Omega,T)+A_{ah}(\Omega,T). \quad (4)$$

Here we work entirely within the quasiharmonic approximation, where $A_{ah}=0$ and the phonons interact only weakly and are determined by zero-temperature forces. Anharmonic effects will be considered in our subsequent second paper, but any additional electron-phonon coupling is neglected. The familiar result for the remaining quasiharmonic phonon free energy can be written

$$A_{qh}(\Omega,T)=\frac{1}{N}\sum_{\kappa}\left[\frac{1}{2}\hbar\,\omega_\kappa+k_BT\ln\{1-e^{-\hbar\omega_\kappa/k_BT}\}\right], \quad (5)$$

where k_B is Boltzmann's constant and ω_κ represents an individual phonon frequency. The summation is over $\kappa=\mathbf{k}s$, where a regular k-point mesh of the irreducible part of the Brillouin zone is used and where s represents the individual phonon branches. It should be noted that in general ω_κ is dependent on volume, but not on temperature.

With this partitioning of the Helmholtz free energy, the individual contributions to the isothermal elastic moduli, C^T_{ijkl}, are calculated by taking the strain derivatives on Eq. (1). With the displacement given as $\mathbf{u}=\mathbf{X}-\mathbf{x}$, between the reference configuration $\mathbf{X}$ and the strained configuration $\mathbf{x}$, the displacement gradient is then given by $u_{ij}=\partial u_i/\partial X_j$ and the Lagrangian strains are $\eta_{ij}=\frac{1}{2}(u_{ij}+u_{ji}+\Sigma_k u_{ki}u_{kj})$. Thus, the derivative with respect to the strain on the Helmholtz energy, Eq. (1), is

$$C^T_{ijkl}=\frac{1}{\Omega}\left.\frac{\partial^2 A}{\partial\eta_{ij}\,\partial\,\eta_{kl}}\right|_{T\eta'}, \quad (6)$$

where η' indicates that all other strains are held fixed. This yields the individual cold, electron-thermal, and ion-thermal, contributions to the elastic moduli:

$$C^T_{ijkl}=C^0_{ijkl}+C^{\rm el}_{ijkl}+C^{\rm ion}_{ijkl}. \quad (7)$$

In general, for a material under a hydrostatic pressure P, as represented by a stress tensor $\tau^0_{ij}=-P\delta_{ij}$, the stress-strain coefficients B^T_{ijkl} defined by Wallace[17] according to

$$\tau_{ij}(\mathbf{x},T)=\tau^0_{ij}(\mathbf{X},T)+\sum_{kl}B^T_{ijkl}\eta_{kl}+\cdots \quad (8)$$

are the most convenient quantities to consider. The coefficients B_{ijkl} and C_{ijkl} are related through the general expression

$$B_{ijkl}=\frac{1}{2}(\tau_{il}\delta_{jk}+\tau_{jl}\delta_{ik}+\tau_{ik}\delta_{jl}+\tau_{jk}\delta_{il}-2\tau_{ij}\delta_{kl})+C_{ijkl}, \quad (9)$$

which is equally valid for either isothermal or adiabatic moduli. For cubic materials, where there are three independent elastic moduli at a given volume or pressure, this expression yields the well-known relationships (in Voigt notation) $B_{11}=C_{11}-P$, $B_{12}=C_{12}+P$, and $B_{44}=C_{44}-P$. In the high-pressure physics community, it is customary to refer to the B_{ijkl} as the pressure-dependent elastic moduli of the material and indeed to denote them as C_{ijkl}. Here we retain the Wallace notation defined above for clarity. Physically, the C_{ijkl} are elastic moduli with the reference system taken as the *uncompressed* perfect crystal at its equilibrium volume Ω_0 and zero pressure, whereas the B_{ijkl} are the moduli with the reference system taken as the *compressed* perfect crystal at volume Ω and pressure P. The B_{ijkl} thus have the same interpretation at each volume or pressure considered.

To compare with experiment, the isothermal moduli B^T_{ijkl} must also be transformed to the adiabatic moduli B^S_{ijkl} by the following relation:

$$B^S_{ijkl}-B^T_{ijkl}=\frac{T\Omega}{C_\eta}\left.\frac{\partial\tau_{ij}}{\partial T}\right|_\eta\left.\frac{\partial\tau_{kl}}{\partial T}\right|_\eta, \quad (10)$$

noting that $B^S_{ijkl}-B^T_{ijkl}=C^S_{ijkl}-C^T_{ijkl}$. For an isotropic material this relationship is simplified, since the stress tensor is $\tau_{ij}=-P\delta_{ij}$. Also, C_η can be replaced by C_V, the specific heat at constant volume, for cubic materials under hydrostatic pressure. In this case Eq. (10) leads to the useful results (in Voigt notation)

$$B_{44}=B^S_{44}=B^T_{44} \quad (11)$$

and

$$B^S_{11}-B^T_{11}=B^S_{12}-B^T_{12}=\frac{T\Omega}{C_V}\beta^2B_T^2, \quad (12)$$

where β is the usual thermal expansion coefficient $\beta=\Omega^{-1}\partial\Omega/\partial T|_P$ and B_T is the isothermal bulk modulus $B_T=\Omega\,\partial P/\partial\Omega|_T=\frac{1}{3}(B_{11}+2B_{12})$. From Eq. (12), it follows that the adiabatic bulk modulus is just

$$B_S=B_T+\frac{T\Omega}{C_V}\beta^2B_T^2 \quad (13)$$

and that the shear modulus $B'=\frac{1}{2}(B_{11}-B_{12})$ is that same for either the isothermal or adiabatic case. At zero pressure, of course, B' and B_{44} reduce to C' and C_{44}, respectively, and the familiar notation for the shear moduli is recovered.

In practice we determine the three independent isothermal moduli B^T_{ijkl} and their components at a given volume and temperature from the bulk modulus B_T via the equation of

state, Eq. (2), corresponding to a pure volume deformation of the metal, and from the shear moduli B' and B_{44} via volume-conserving tetragonal and orthorhombic deformations.[7,23]

B. Computational methods

The cold and electron-thermal contributions to the elastic moduli of our Ta prototype are calculated from first principles using the FP-LMTO method.[7,20] This all-electron, full-potential DFT method is very robust, and in the past it has been successfully applied to calculate the structural, mechanical, and defect properties of many *d*-transition metals including Ta.[7,14,24] Here, we build on previous FP-LMTO Ta calculations of the cold elastic moduli to 10 Mbar in pressure[7] and use the same computational prescription but with the inclusion of temperature. In this approach, all relativistic effects are included: the core electrons are treated by solving the Dirac equation and the spin-orbit interaction is accounted in a variational fashion for the valence states.[25] This is a full-potential method that does not have any shape approximations to either the one-electron potential or to the charge density. This is accomplished by dividing the crystal into two regions: muffin-tin spheres surrounding each atom and the remaining interstitial volume. Within the spheres, centered at each atomic site and moving rigidly with the atom under deformation, a Bloch sum of linear-muffin-tin orbitals and an expansion in terms of structural constants describe the wave functions. In the interstitial region, the wave functions are expanded in Hankel and Neumann functions and with Bessel functions. Also, in the interstitial region, the kinetic energy can be nonzero and is described by a double-basis set for the semicore states $5s$, $5p$, and $4f$ and for the valence states $6s$, $6p$, $5d$, and $5f$ (the use of the double basis reduces truncation errors in the expansions). For the exchange-correlation functional in DFT, the generalized gradient approximation (GGA) by Perdew *et al.*[26] is used. The electron temperature is incorporated through the Fermi-Dirac distribution as previously mentioned, and the electronic entropy is calculated via Eq. (3). The free energy calculations for Ta are well converged to the μRy level, where approximately 2000 k points over the irreducible part of the Brillouin zone for the smallest of volumes was determined to be satisfactory. For each volume considered (seven volumes total), the shear elastic moduli B' and B_{44} were calculated for seven to nine temperatures. In each case this was accomplished by calculating the free energy as a function of shear strain relative to the compressed lattice and then fitting the result with a suitable quadratic function to extract the cold plus electron-thermal modulus.

The remaining ion-thermal contribution to the Ta elastic moduli is calculated with the complementary MGPT multi-ion potentials derived from DFT-based generalized pseudopotential theory.[18,19] The MGPT potentials fully account for the directional bonding arising from partially filled *d* bands in central transition metals, which is important to the reliable calculation of structural and mechanical properties in these materials. For the bulk metal at volume Ω, the GPT total-energy functional that defines the potentials is of the form

$$E_{\mathrm{tot}}(\mathbf{R}_1,\ldots,\mathbf{R}_N) = NE_{\mathrm{vol}}(\Omega) + \frac{1}{2}{\sum_{i,j}}' v_2(ij;\Omega) + \frac{1}{6}{\sum_{i,j,k}}' v_3(ijk;\Omega) + \frac{1}{24}{\sum_{i,j,k,l}}' v_4(ijkl;\Omega), \tag{14}$$

where $\mathbf{R}_1,\ldots,\mathbf{R}_N$ denotes the positions on the N ions in the metal and the prime on each sum over ion positions excludes all self-interaction terms where two indices are equal. The leading volume term in this expansion, E_{vol}, as well as the two-, three-, and four-ion interatomic potentials v_2, v_3, and v_4, are volume-dependent, but *structure-independent* quantities and thus *transferable* to all bulk ion configurations, either ordered or disordered, including the deformed solid. For the perfect bcc solid, $E_{\mathrm{tot}}=E_0$, the cold energy in Eq. (1). In Eq. (14), the ion-ion pair potential $v_2(ij;\Omega)=v_2(R_{ij},\Omega)$ at fixed volume is a one-dimensional function of the radial distance R_{ij} between the ion sites i and j. The three- and four-ion potentials are the corresponding three and six-dimensional functions, $v_3(ijk;\Omega)=v_3(R_{ij},R_{jk},R_{ki},\Omega)$ and $v_4(ijkl;\Omega)=v_4(R_{ij},R_{jk},R_{kl},R_{li},R_{ki},R_{lj},\Omega)$, respectively. In the full first-principles GPT, these are all long-ranged nonanalytic functions, however, so that the multi-ion potentials v_3 and v_4 cannot be readily tabulated for application purposes. This has led to the development of the model GPT or MGPT for bcc transition metals.[19] Within the MGPT, the multi-ion potentials are systematically approximated by introducing canonical *d* bands and other simplifications to achieve short-ranged analytic forms, which can then be applied to both static and dynamic simulations. To compensate for the approximations introduced into the MGPT, a limited amount of parametrization is allowed in which the volume-dependent coefficients of the modeled potential contributions are constrained by first-principles theoretical data on fundamental quantities or, if desired and available, the corresponding experimental data. In this form, the MGPT has proven to provide a robust framework for performing accurate and predictive atomistic simulations on bulk transition metals.

In the present work, we have used the optimized Ta MGPT potentials recently developed for application to structural, thermodynamic, defect, and mechanical properties in the 0–10-Mbar pressure range.[13,15] The constraining physical data in this case have been obtained from our first-principles FP-LMTO calculations,[7,14] augmented by a small amount of experimental data near ambient conditions. As a consequence the present MGPT potentials are highly consistent with the FP-LMTO results and, in particular, well reproduce the cold equation of state and the cold shear moduli over the entire 10-Mbar pressure range. The latter comparison is shown in Fig. 1. In addition, the potentials yield good phonons over this same pressure range, with the prediction of a Grüneisen parameter with a nonlinear volume dependence.[13] The Ta MGPT potentials also have been successfully applied to many related problems, including melting and resolidification, point-defect formation and migration, dislocation structure and mobility, and grain-boundary structure.[13,15,27]

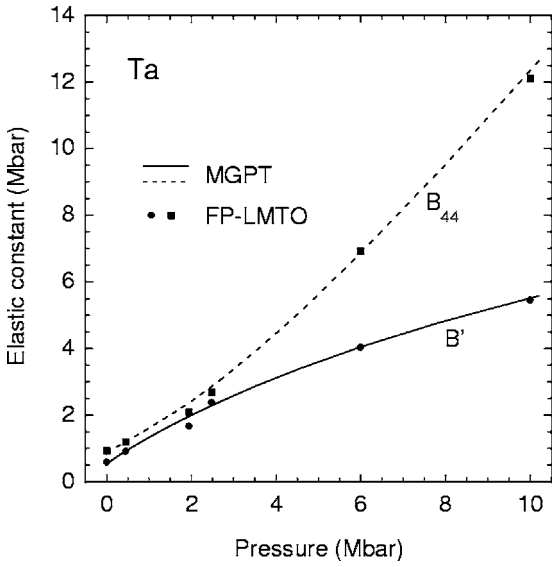

FIG. 1. Zero-temperature shear elastic moduli in bcc Ta over the 10-Mbar pressure range of interest in this paper, as calculated from the FP-LMTO method and from the present MGPT multi-ion interatomic potentials.

The ion-thermal contribution to C^T_{ijkl} in Eq. (7) is obtained from the strain differentiation of $A_{qh}(\Omega,T)$, which can be written as the Brillouin-zone summation

$$C^{\rm ion}_{ijkl}=\frac{1}{\Omega}\sum_{\kappa}\hbar\,\omega_{\kappa}\left\{\xi_{\kappa,ijkl}\left[\bar{n}_{\kappa}+\frac{1}{2}\right]+\gamma_{\kappa,ij}\gamma_{\kappa,kl}T\left.\frac{\partial\bar{n}_{\kappa}}{\partial T}\right|_{\eta}\right\}, \tag{15}$$

where $\bar{n}_{\kappa}=(e^{-\hbar\omega_{\kappa}/k_BT}-1)^{-1}$ is the Bose-Einstein distribution and the strain derivatives of the phonon frequencies are defined as

$$\gamma_{\kappa,ij}=-\frac{1}{\omega_{\kappa}}\left.\frac{\partial\omega_{\kappa}}{\partial\eta_{ij}}\right|_{\eta'}, \tag{16}$$

$$\xi_{\kappa,ijkl}=\frac{1}{\omega_{\kappa}}\left.\frac{\partial^2\omega_{\kappa}}{\partial\eta_{ij}\partial\eta_{kl}}\right|_{\eta'}. \tag{17}$$

Again η' means that all other strains are held fixed. The quantity $\gamma_{\kappa,ij}$ is the generalized Grüneisen parameter. In principle, these derivatives can be obtained by formal strain differentiation of the dynamical matrix, but here this is a formidable task due to the complex many-body nature of the MGPT total energy, Eq. (14). Therefore, we have instead developed a numerical procedure to evaluate the quantities $\gamma_{\kappa,ij}$ and $\xi_{\kappa,ijkl}$ by expanding ω_{κ} in powers of η_{ij},

$$\omega_{\kappa}(\mathbf{x},\eta_{ij})=\omega_{\kappa}(\mathbf{X})+\sum_{ij}a_{\kappa,ij}\eta_{ij}+\sum_{ijkl}b_{\kappa,ijkl}\eta_{ij}\eta_{kl}+\cdots, \tag{18}$$

where the expansion coefficients $a_{\kappa,ij}$ and $b_{\kappa,ijkl}$ are proportional to the desired quantities $\gamma_{\kappa,ij}$ and $\xi_{\kappa,ijkl}$, respectively. In this procedure, ω_{κ} is calculated for a series of small deformations in an analogous manner to that of determining the zero-temperature elastic moduli. The result is then fitted with Eq. (18) and the expansion coefficients obtained. For a cubic system, volume-conserving orthorhombic and tetragonal deformations, as well as a uniform compression of the system, give useful combinations of the expansion coefficients from which $\gamma_{\kappa,ij}$ and $\xi_{\kappa,ijkl}$ can be obtained and the ion-thermal elastic moduli calculated via Eq. (15). For the Brillouin-zone summation in Eq. (15), we have found no change in results for a regular k-point mesh of more than 500 points. Ion-thermal components to the Ta elastic moduli were thereby calculated at a total of 18 volumes with at least 40 temperature points for each volume.

TABLE I. The present calculated adiabatic elastic moduli in Ta at ambient conditions ($P=0$, $T=300$ K) compared to experimental data, with all quantities in Mbar. Note $C^S_{44}=C^T_{44}=C_{44}$.

	C^S_{11}	C^S_{12}	C^S_{44}	C'	B_S
Present theory	2.58	1.55	0.74	0.52	1.89
Katahara *et al.*[a]	2.66	1.61	0.82	0.53	1.96
Featherston and Neighbours[b]	2.61	1.57	0.82	0.52	1.92
Cynn and Yoo[c]	2.47	1.76	0.84	0.36	2.00
Cynn and Yoo[d]					1.94

[a]Reference 29.
[b]Reference 30.
[c]Reference 3.
[d]Reference 12.

III. RESULTS AND COMPARISONS

In this section we discuss our calculated results, with an emphasis on comparison with experiment at both ambient and extreme conditions and on making contact with the impact of thermoelasticity on constitutive strength modeling. As has been indicated, the calculations of the cold, electron-thermal, and ion-thermal components of the Ta elastic moduli and pressure were performed over individual grids of volume and temperature via the aforementioned FP-LMTO and MGPT methods. These separate contributions were then brought together through interpolation for each Ω,T point of interest, using Birch-Murnaghan-type[28] fits in the volume Ω and polynomial fits in the temperature T. As above, the notation C_{ijkl} will be used for $P=0$ and B_{ijkl} when $P\neq 0$ in the general case, while specific elastic moduli will be written in contracted Voigt notation.

A. T and P dependence

We first consider the temperature and pressure dependence of the single-crystal Ta elastic moduli. Our adiabatic elastic moduli at ambient pressure and temperature conditions are given in Table I and compared with experimental data from several sources. The latter include accurate ultrasonic measurements[29,30] as well as high-pressure diamond-anvil-cell (DAC) measurements extrapolated to zero pressure. The DAC results for C^S_{ijkl} were obtained by a stress and angle-resolved x-ray diffraction (SAX) technique[3] and in the case of the bulk modulus also from independent DAC

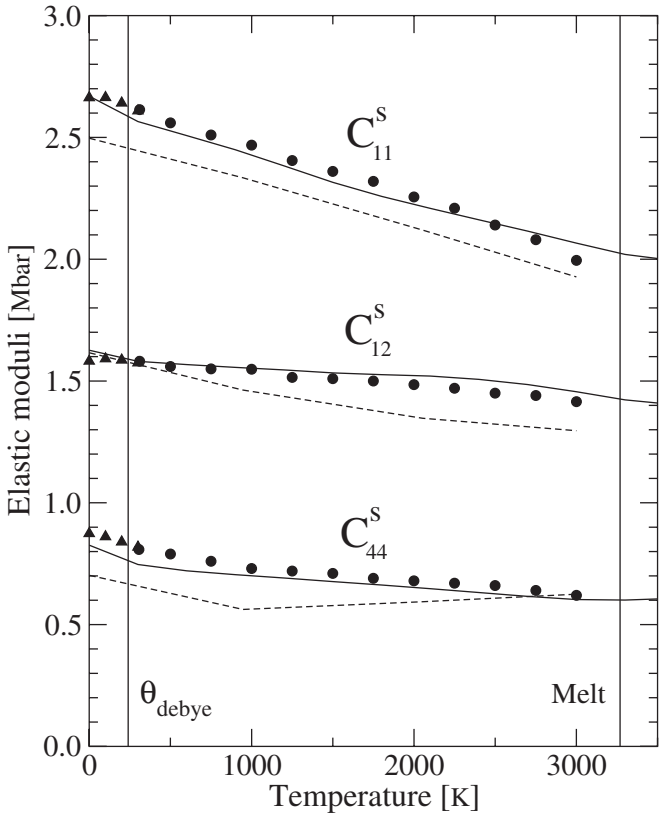

FIG. 2. For single-crystal Ta at ambient pressure, the present calculated adiabatic elastic moduli (solid lines) and corresponding ultrasonic data (Refs. 4 and 30) (solid circles and triangles) are compared as a function of temperature up to melt. Previous calculations via the PIC method (Ref. 10) (dashed lines) are also shown. Note that $C^S_{44}=C^T_{44}=C_{44}$ and that $C^S_{11}>C^S_{12}>C^S_{44}$ at all temperatures, which is consistent with bcc lattice stability up to melt.

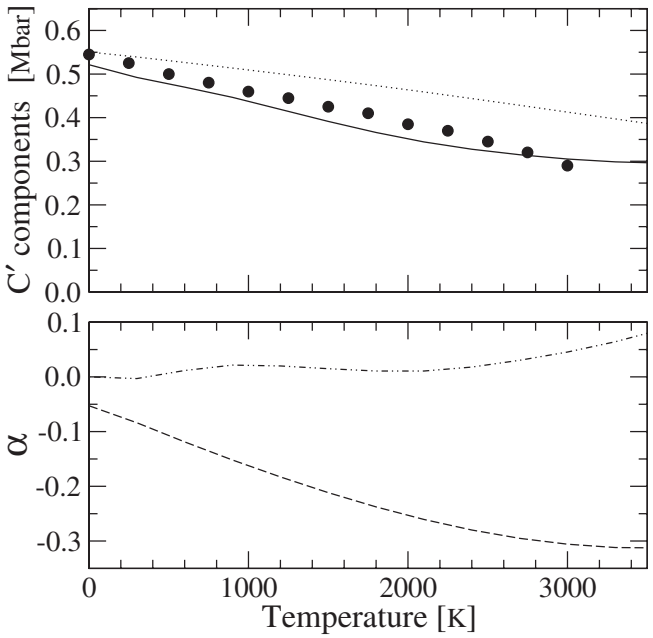

FIG. 3. The present calculated Ta shear modulus C' and its components as a function of temperature at ambient pressure. Top panel: the full calculated C' (solid line) and its cold component (dotted line) together with experimental data (Ref. 4) (solid circles). Bottom panel: the relative electron-thermal (dot-dashed line) and ion-thermal (dashed line) components to C', as defined in Eq. (19).

equation-of-state measurements.[12] It should be noted that the DAC-SAX results have significantly larger error bars than the other data. Our calculated results are in generally good accordance with ultrasonic data, with the largest discrepancy being a 10% underestimate in the value of C^S_{44}.

For the temperature dependence of the Ta elastic moduli, we present in Fig. 2 our calculated results in the range 0–3500 K at ambient pressure together with data taken from ultrasonic measurements.[4,30] The overall agreement of the present results with experiment is very good at all temperatures, even near melt. Both theory and experiment indicate significant thermal softening in C^S_{11} and C^S_{44} at high temperature. As discussed below, the overall observed trend towards softening of the elastic moduli at high T is due to thermal expansion—i.e., the decrease in the cold contribution C^0_{ijkl} with increasing volume—but the electron- and ion-thermal contributions play significant quantitative roles in their detailed behavior. In particular, the anomalous temperature behavior of C^S_{44} (non-T^4 decrease for low T and non-T decrease for high T) discussed in Ref. 4 is obtained in our calculations. Also plotted in Fig. 2 for comparison are the Ta elastic moduli calculated by Gülseren and Cohen [10] with their PIC method.

To provide further insight into the thermal dependence of the Ta elastic moduli, we present in Figs. 3 and 4 the separate cold, electron-thermal, and ion-thermal contributions to the shear moduli C' and C_{44}. For this purpose, we have factored the cold component C^0_{ijkl} from Eq. (7) obtaining the thermal components to C_{ijkl} as relative fractions $\alpha^{\rm el}_{ijkl}=C^{\rm el}_{ijkl}/C^0_{ijkl}$ and $\alpha^{\rm ion}_{ijkl}=C^{\rm ion}_{ijkl}/C^0_{ijkl}$ to the cold component, so that

$$C_{ijkl}=C^0_{ijkl}(1+\alpha^{\rm el}_{ijkl}+\alpha^{\rm ion}_{ijkl}). \tag{19}$$

These definitions can be applied to either isothermal or adiabatic moduli and likewise to B_{ijkl}. In C' as well as C_{44}, the cold component to the modulus (top panels of Figs. 3 and 4) contributes a major part of the high-temperature softening. This directly reflects the thermal volume expansion required to maintain zero pressure. In both cases, however, the electron- and ion-thermal components are equally important to the overall thermal dependence of the modulus. Interestingly, the roles of the two thermal components interchange in their importance in the two cases. For C' (bottom panel of Fig. 3) the ion-thermal component is a factor of 3 larger in value than the electron-thermal component and is negative, thus helping to soften C' near melt, whereas for C_{44} (bottom panel of Fig. 4) the electron-thermal component increasingly contributes to the overall softening of that modulus as melt is approached. It is primarily the electron-thermal component that is responsible for driving C_{44} away from its expected T^4 low-temperature behavior and T high-temperature behavior.

We next turn to comparisons with experiment at high pressure and high temperature. In Fig. 5 we compare our calculated high-pressure adiabatic moduli B^S_{ijkl} at 300 K with room-temperature data obtained from DAC-SAX measurements to 1.05 Mbar (105 GPa).[3] Over this pressure range

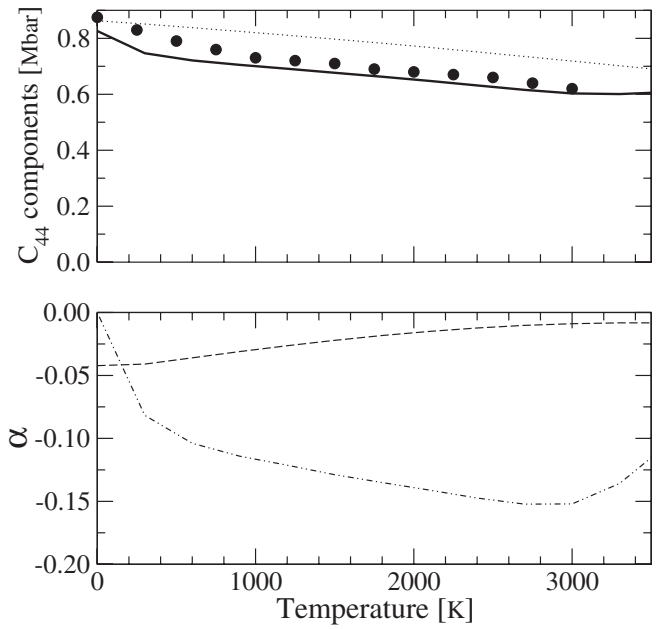

FIG. 4. The present calculated Ta shear modulus C_{44} and its components as a function of temperature at ambient pressure. Top panel: the full calculated C_{44} (solid line) and its cold component (dotted line) together with experimental data (Ref. 4) (solid circles). Bottom panel: the relative electron-thermal (dot-dashed line) and ion-thermal (dashed line) components to C_{44}, as defined in Eq. (19). Note the rapid negative increase in the electron-thermal contribution below 500 K and the corresponding rapid decrease above 3000 K, which explain the observed anomalous thermal behavior of C_{44} discussed in the text.

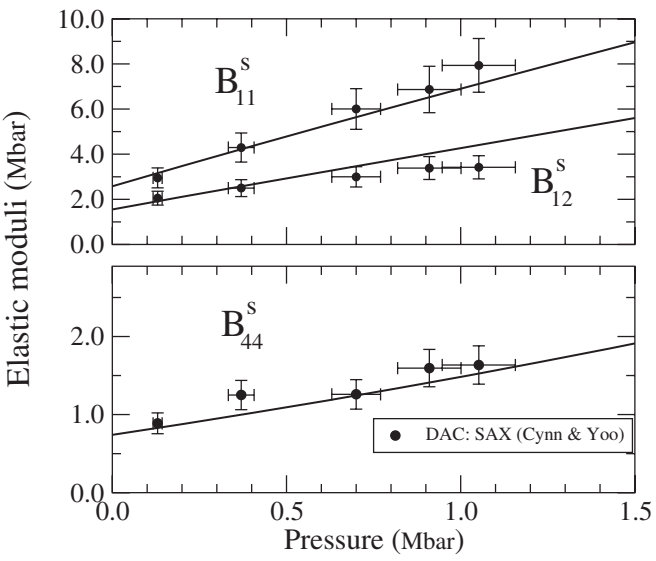

FIG. 5. The present calculated high-pressure elastic moduli B^S_{ijkl} compared to DAC-SAX data (Ref. 3) as a function of pressure at $T=300$ K.

and up to about 2 Mbar, we predict linear dependences of B^S_{11}, B^S_{12}, and B^S_{44} on pressure that appear consistent with the data, although the error bars in DAC-SAX measurements become quite large above 0.7 Mbar.

At higher pressures and temperatures in Ta, contact with shock experiments can be made through the measured sound velocity,[22] which can be obtained in both the bulk solid and the liquid and is frequently used as a diagonstic to detect shock melting. In such an experiment, the sound velocity of a macroscopic, polycrystalline sample is measured along the Hugoniot of the material, which is a locus of final shock states reached from a common initial state (P_0, T_0). To determine the principal Hugoniot, which is the path of interest here, it is sufficient to take $P_0=0$ and $T_0=300$ K, and to calculate the Hugoniot path in pressure and temperature from the FP-LMTO- and MGPT-derived Ta equation of state.[13] The adiabatic moduli $B^S_{ijkl}(P,T)$ can then be calculated along the same path and used to estimate the isotropic, polycrystalline aggregate sound speed for Ta through the bulk modulus B_S and average shear modulus G.[8,10,17] The latter is here obtained by averaging the rigorous Hashin-Shtrikman bounds g_1 and g_2 for an isotropic polycrystal:[21]

$$G = \frac{1}{2}(g_1 + g_2), \tag{20}$$

where

$$g_1 = B' + \frac{3}{\dfrac{5}{B_{44} - B'} - 4\beta_1},$$

$$g_2 = B_{44} + \frac{2}{\dfrac{5}{B' - B_{44}} - 6\beta_2}, \tag{21}$$

with

$$\beta_1 = -3\frac{B_S + 2B'}{5B'(3B_S + 4B')},$$

$$\beta_2 = -3\frac{B_S + 2B_{44}}{5B_{44}(3B_S + 4B_{44})}. \tag{22}$$

Our calculated longitudinal sound velocity $v_{\text{long}} = \sqrt{(B_S + 4G/3)/\rho}$, where ρ is the density, is plotted in Fig. 6, for the bcc solid and is seen to coincide well with the solid phase shock data.[22] Near 3 Mbar the measured sound velocity drops to its bulk value, $v_{\text{bulk}} = \sqrt{B_S/\rho}$, which is the value attained when the shear moduli G goes to zero as the bcc solid melts and transforms to a liquid. In Fig. 6 our calculated bulk sound velocity is that for the solid bcc phase rather than the liquid, but good agreement with the data is maintained. In this regard, the difference between the solid and liquid bulk moduli in Ta is expected to be small, since the volume change at the calculated shock melt temperature of approximately 11 000 K is only a few percent. Hence, we expect only small changes to the bulk sound velocity above the shock melt point. Additionally, for comparison, the calculated shear sound velocity, $v_{\text{shear}} = \sqrt{G/\rho}$, in the bcc solid is plotted in Fig. 6.

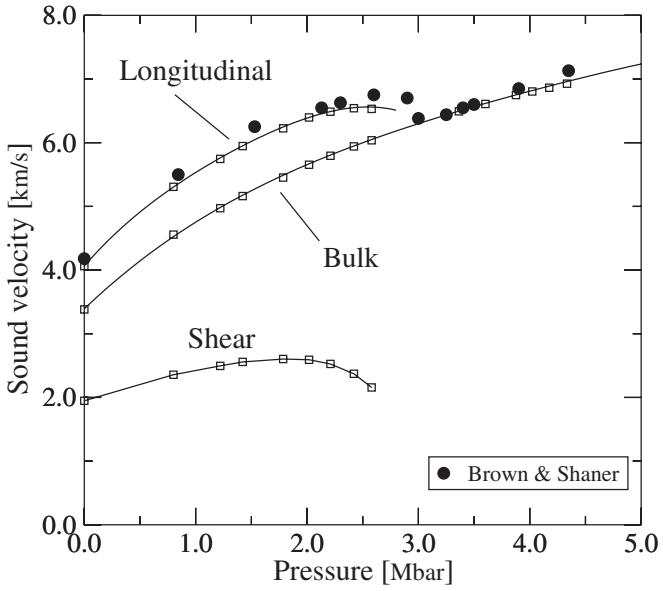

FIG. 6. Longitudinal, bulk, and shear sound velocity in Ta along its principal Hugoniot. Present results: open squares and solid line fits to the calculated points for the bcc polycrystal based on the bulk modulus B_S and the average shear modulus G obtained from Hashin-Shrikman bounds. Experimental data from Ref. 22: solid points. The sharp drop in measured sound velocity near 3 Mbar is indicative of shock melting, where the shear modulus G has dropped to zero in the liquid above that point.

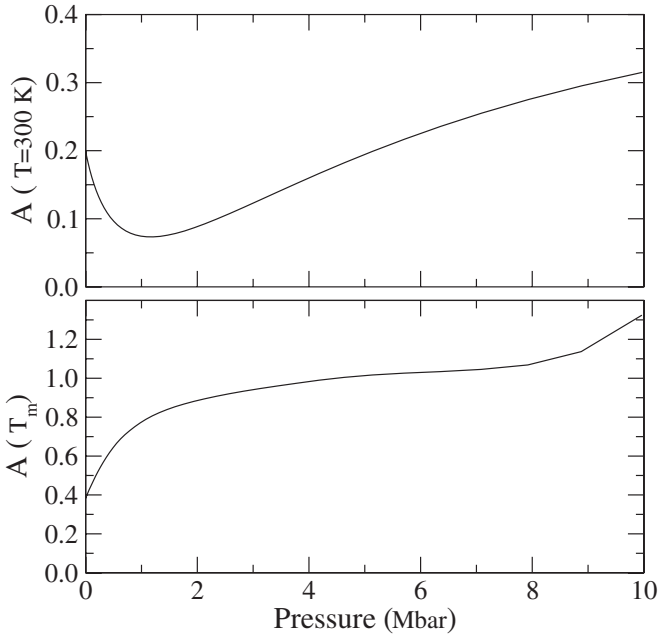

FIG. 7. The pressure dependence of the single-crystal elastic anisotropy is shown for the $T=300$ K isotherm (top) and along the melt curve T_m (bottom). The minimum in A at $T=300$ K and 1 Mbar (top) is removed by the electron and ion thermal components at high temperature along the melt.

A related measure relevant to the sound velocities for single crystals is the elastic anisotropy ratio A. Here we use the definition[8] $A=2(B_{44}-B')/B_{11}$ for a cubic system. For bcc tantalum we give in Fig. 7 (top) the pressure dependence of $A(P,T=300\ \mathrm{K})$, where it is seen that there is a rapid decrease in value until approximately 1 Mbar then A increases to over 0.3 at 10 Mbar. This is qualitatively similar to previous tantalum results at $T=0$ K for the ratio B_{44}/B' obtained by FP-LMTO and also by MGPT calculations.[13] At ambient conditions the present theory yields a ratio of $A=0.20$, which compares well to the experimental ratio of $A=0.22$ based on data of the Katahara *et al.*[29] While the DAC-SAX data[3] confirm the initial decrease in A with pressure, a close comparison between theory and experiment is not possible, because the error bars for the data (not shown in Fig. 7) are large. Also given in Fig. 7 (bottom) is the anisotropic ratio along the melt line. The theoretical melt line extends from $T=3400$ K at $P=0$ to $T=26\,000$ K at $P=10$ Mbar. Electron- and ion-thermal effects stiffen B_{44} relative to B' and remove the minimum seen in the top panel, so that A is significantly increased at all pressures. This behavior is detailed below in terms of the individual moduli along the melt.

As a final example of predicted thermoelastic behavior in Ta, we consider the behavior of the single-crystal bcc shear elastic moduli B' and B_{44} along the high-pressure melt curve. In Fig. 8 we plot our calculated shear elastic moduli and their components along this path. It is seen that B_{44} increases more or less linearly with pressure, which is similar to its behavior at low temperature. In contrast, B' decreases monotonically with pressure, becoming negative beyond about 1 Mbar. This behavior is driven by the large negative ion-thermal contribution calculated in the quasiharmonic limit. However, full molecular dynamics (MD) simulations of the high-temperature solid with the same MGPT potentials[13] demonstrate that the bcc structure is everywhere stable up to melt. Since the MD simulations implicitly include anharmonic effects, this implies that B' should remain everywhere positive and that here there are large missing anharmonic contributions. These latter contributions are currently being investigated with our full MC-MGPT approach to be reported in our subsequent second paper.

B. Implications for constitutive modeling

In this section we briefly discuss the implications of our advanced treatment of thermoelasticity on constitutive models of strength. Such models typically scale the strength at ambient conditions to high pressure and temperature through the average shear modulus $G(P,T)$. In particular, this is done very explicitly in the well-known and widely used Steinberg-Guinan (SG) strength model.[2] The SG model includes a phenomenological relation for $G(P,T)$ appropriate to macroscopic polycrystalline material that is essentially a modified Taylor series expansion to first order in both pressure and temperature:

$$G(P,T)=G_0\left[1+\frac{1}{G_0}\frac{dG}{dP}\frac{P}{\eta^{1/3}}+\frac{1}{G_0}\frac{dG}{dT}(T-300)\right], \quad (23)$$

where $G_0=G(P=0,T=300\ \mathrm{K})$ and where $\eta=\Omega/\Omega_0$. The assumed pressure dependence in Eq. (23) has been previously validated in the case of Ta to about 6 Mbar using our first-principles FP-LMTO results.[7] Here we focus only on the

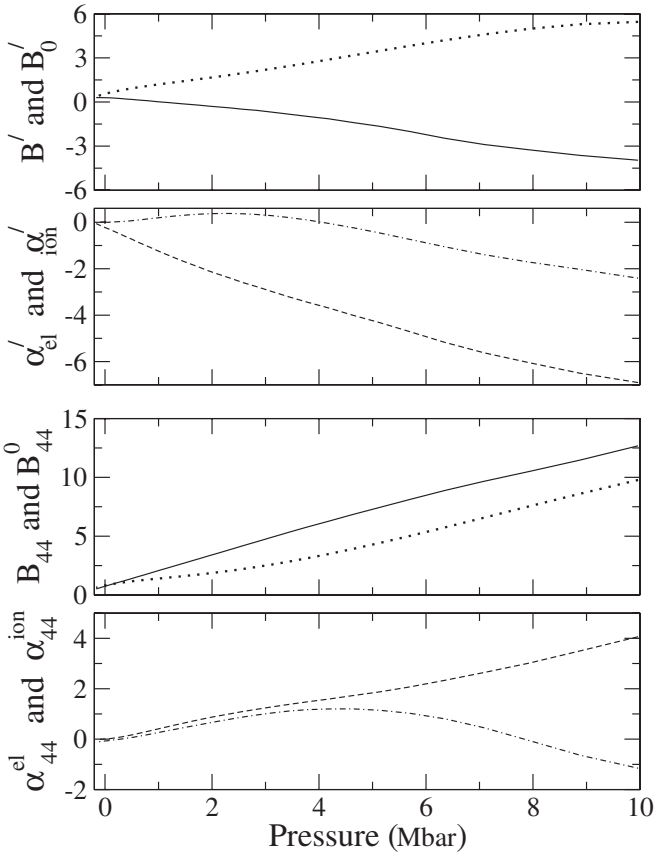

FIG. 8. High-pressure and -temperature shear elastic moduli and their components in bcc Ta, as calculated along the melt curve to 10 Mbar. The temperature range along the melt line is from 3400 K at ambient to 26 000 K at 10 Mbar (Ref. 13). The top panel displays B' (solid line) and its cold component B'_0 (dotted line). The second panel from the top shows the additional electron- and ion-thermal relative components $\alpha'_{\rm el}$ (dot-dashed line) and $\alpha'_{\rm ion}$ (dashed line). The third and fourth panels from the top display the corresponding results for B_{44} and its components. Note that B' becomes negative beyond about 1 Mbar in pressure.

temperature dependence contained in the final term of Eq. (23). Specifically, we consider $G(P=0,T)=G_0[1+A_0(T-300)]$, where $A_0=1/G_0(dG/dT)$ is evaluated at zero pressure and $T=300$ K. Using the present single-crystal elastic moduli, we have calculated the corresponding Voigt average $G_{\rm v}(0,T)=1/5[2C'(0,T)+3C_{44}(0,T)]$ and compared the result with SG in Fig. 9. (Using the alternative Hashin-Shtrikman average of the shear modulus considered above, we obtain similar results.) The ambient-temperature shear modulus G_0 used in the SG model for Ta has an empirical value of 0.69 Mbar, while we calculate 0.64 Mbar, reflecting our underestimate of C_{44} from Table I. For A_0, the SG model gives -0.13 $[\mathrm{kK}]^{-1}$ compared to our calculated value of -0.10 $[\mathrm{kK}]^{-1}$. As shown in Fig. 9, the SG model describes the overall linear trend of the experimental data from near the Debye temperature (226 K) to about 1500 K, corresponding to about half of the melt temperature. However, below 200 K and above 1500 K both experiment and the present theory indicate a significant departure from a linear temperature dependence for $G(0,T)$.

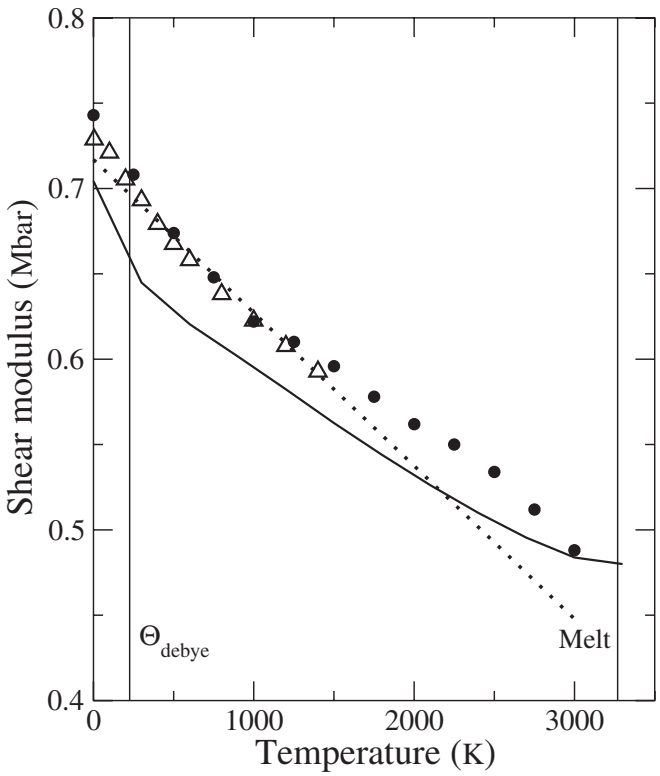

FIG. 9. Temperature dependence of the average shear modulus in Ta at ambient pressure, as applicable to constitutive models of strength. Included for comparison are the Steinberg-Guinan model (Ref. 2) (dotted line) and the present Voigt average of single-crystal bcc moduli (solid line) together with experimental data (open triangles and solid circles). The open triangles represent polycrystalline data from Ref. 5 while the solid circles are Voigt-averaged single-crystal data (Ref. 4).

The linear temperature dependence of $G(P,T)$ assumed in the SG model is a common assumption that is widely used in analytical modeling of the shear modulus.[31,32] If a more accurate description is required, then a full calculation such as that presented here must be performed, where both the electron- and ion-thermal contributions are taken into account. This leads one away from simple analytical models but to equally tractable, tabular representations of the elastic moduli.

IV. CONCLUSIONS

We have presented in this paper an approach to thermoelasticity for transition metals that self-consistently combines a first-principles FP-LMTO treatment of cold and electron-thermal components of elastic moduli with a quantum-based MGPT treatment of the ion-thermal component. Here the latter has been developed entirely within the quasiharmonic phonon approximation, leading to a very computationally efficient method that is applicable to materials and/or temperature-pressure regimes where anharmonic effects are small. As a prototype, we have extensively applied this approach to bcc tantalum over wide ranges of temperature and pressure, up to 26 000 K at 10 Mbar. In this

regard, we have demonstrated through comparison with experiment that the method well describes (i) the temperature dependence of the single-crystal elastic moduli at ambient pressure all the way to melt, including anomalous nonlinear behavior at low and high temperatures; (ii) the pressure dependence of the elastic moduli at ambient temperature to above 1 Mbar; and (iii) longitudinal and bulk sound velocities of the polycrystal along the Hugoniot up to and including shock melting near 3 Mbar. At the same time, we find that the B' shear modulus becomes negative at high temperature along the melt curve above 1 Mbar in pressure. Since full MD simulations (where anharmonicity is implicitly treated) indicate that the bcc structure remains everywhere mechanically stable, we conclude that anharmonic contributions to the thermoelasticity become important in this regime. These missing anharmonic effects will be treated in our more general MC-MGPT ion-thermal approach to be reported in a subsequent paper of this series. Finally, in the context of constitutive strength models, we have validated the assumed linear temperature dependence of the shear modulus $G(P,T)$ for Ta in the range extending from the Debye temperature to the half of the melt temperature. In the future it should be possible to use general treatments of thermoelasticity such as the present one to develop more accurate models of $G(P,T)$ for high-pressure and -temperature constitutive modeling applications, as required.

ACKNOWLEDGMENTS

We would like to thank J. E. Klepeis for helpful discussions. This work was performed under the auspices of the U.S. Department of Energy by the University of California Lawrence Livermore National Laboratory under Contract No. W-7405-Eng-48.

[1] J. A. Moriarty, V. Vitek, V. V. Bulatov, and S. Yip, J. Comput.-Aided Mater. Des. **9**, 99 (2002).
[2] D. J. Steinberg, S. G. Cochran, and M. W. Guinan, J. Appl. Phys. **51**, 1498 (1980); D. J. Steinberg and C. M. Lund, *ibid.* **65**, 1528 (1989).
[3] H. Cynn and C.-S. Yoo (unpublished).
[4] E. Walker and P. Bujard, Solid State Commun. **34**, 691 (1980).
[5] H. Wawra, Z. Metallkd. **69**, 518 (1978).
[6] P. Hohenberg and W. Kohn, Phys. Rev. **136**, B864 (1964); W. Kohn and L. Sham, Phys. Rev. **140**, A1133 (1965).
[7] P. Söderlind and J. A. Moriarty, Phys. Rev. B **57**, 10340 (1998).
[8] B. B. Karki, L. Stixrude, and R. M. Wentzcovitch, Rev. Geophys. **39**, 507 (2001).
[9] C. W. Greeff and J. A. Moriarty, Phys. Rev. B **59**, 3427 (1999).
[10] O. Gülseren and R. E. Cohen, Phys. Rev. B **65**, 064103 (2002).
[11] O. Eriksson, J. M. Wills, and D. Wallace, Phys. Rev. B **46**, 5221 (1992).
[12] H. Cynn and C.-S. Yoo, Phys. Rev. B **59**, 8526 (1999).
[13] J. A. Moriarty, J. F. Belak, R. E. Rudd, P. Söderlind, F. H. Streitz, and L. H. Yang, J. Phys.: Condens. Matter **14**, 2825 (2002).
[14] P. Söderlind, L. H. Yang, J. A. Moriarty, and J. M. Wills, Phys. Rev. B **61**, 2579 (2000).
[15] L. H. Yang, P. Söderlind, and J. A. Moriarty, Philos. Mag. A **81**, 1355 (2001).
[16] R. E. Cohen and O. Güseren, Phys. Rev. B **63**, 224101 (2001).
[17] D. C. Wallace, *Thermodynamics of Crystals* (Dover, Mineola, NY, 1998).
[18] J. A. Moriarty, Phys. Rev. B **16**, 2537 (1977); Phys. Rev. B **26**, 1754 (1982); **38**, 3199 (1988).
[19] J. A. Moriarty, Phys. Rev. B **42**, 1609 (1990); **49**, 12431 (1994).
[20] J. M. Wills, O. Eriksson, M. Alouani, and D. L. Price, in *Electronic Structure and Physical Properties of Solids*, edited by H. Dreysse (Springer-Verlag, Berlin, 2000), p. 148.
[21] G. Simmons and H. Wang, *Single Crystal Elastic Constants and Calculated Aggregate Properties: a Handbook*, 2nd ed. (MIT Press, Cambridge, MA, 1971).
[22] J. M. Brown and J. W. Shaner, in *Shock Waves in Condensed Matter—1983*, edited by J. R. Asay *et al.* (Elsevier, New York, 1984), p. 91.
[23] P. Söderlind, O. Eriksson, J. M. Wills, and A. M. Boring, Phys. Rev. B **48**, 5844 (1993).
[24] P. Söderlind, R. Ahuja, O. Eriksson, J. M. Wills, and B. Johansson, Phys. Rev. B **50**, 5918 (1994); P. Söderlind, J. A. Moriarty, and J. M. Wills, *ibid.* **53**, 14063 (1996).
[25] O. K. Andersen, Phys. Rev. B **12**, 3060 (1975).
[26] J. P. Perdew, J. A. Chevary, S. H. Vosko, K. A. Jackson, M. R. Pederson, D. J. Singh, and C. Fiolhais, Phys. Rev. B **46**, 6671 (1992).
[27] J. A. Moriarty, L. X. Benedict, J. N. Glosli, R. Q. Hood, D. A. Orlikowski, M. V. Patel, P. Söderlind, F. H. Streitz, M. Tang, and L. H. Yang, J. Mater. Res. **21**, 563 (2006).
[28] E. Birch, J. Geophys. Res. **83**, 1257 (1978).
[29] K. W. Katahara, M. H. Manghnani, and E. S. Fisher, J. Appl. Phys. **47**, 434 (1976); J. Phys. F: Met. Phys. **9**, 773 (1979).
[30] F. H. Featherston and J. R. Neighbours, Phys. Rev. **130**, 1324 (1963).
[31] D. L. Preston and D. C. Wallace, Solid State Commun. **81**, 277 (1992).
[32] L. Burakovsky, C. W. Greeff, and D. L. Preston, Phys. Rev. B **67**, 094107 (2003).